Article

# Tunable Plasmonic Microcapsules with Embedded Noble Metal Nanoparticles for Optical Microsensing

Céline Burel, Omar Ibrahim, Emanuele Marino, Harshit Bharti, Christopher B. Murray, Bertrand Donnio, Zahra Fakhraai, and Rémi Dreyfus*

Cite This: https://doi.org/10.1021/acsanm.1c04542

Read Online

ACCESS | Metrics & More | Article Recommendations | Supporting Information

**ABSTRACT:** We report a comprehensive investigation of the synthetic conditions leading to the formation of tunable plasmonic microcapsules (MCs) made of a hydrophobic liquid core encapsulated into a hard silica shell embedding plasmonic metallic nanoparticles (NPs). The distinctive and remarkable features of the prepared MCs are the inert nanometer-thin silica shell and the small plasmonic NPs embedded in it, which confer interesting optical absorbance properties. We tie the mechanical robustness of the MCs to the thickness of their silica shell. We show that several oils can be used for the synthesis of MCs and we evidence how the relative solubility of the silica precursor and the polarity of the oil phase influence the final MC characteristics. We also evidence the synthesis of "monoflavor" or "multiflavor" MCs with, respectively, a single type of NPs or a mixture of metallic NPs, respectively, embedded in the silica shell. Using experiments and simulations, we demonstrate that the optical response of the MCs can be finely tuned by choosing the right ratio between Ag and Au NPs initially suspended in the solution. Our heterogeneous hybrid MCs exhibit optical properties directly resulting from the choice of NP composition and shell thickness, making them of great interest not only for mechanical and chemical microsensing but also for applications in photothermal therapy, surface-enhanced Raman spectroscopy studies, microreactor vesicles for interfacial electrocatalysis, antimicrobial activity, and drug delivery. Our simple and versatile emulsion template method holds great promise for the tailored design of a generation of multifunctional MCs consisting of modular nanoscale building blocks.

**KEYWORDS:** microcapsules, nanoparticles, plasmon coupling, emulsion, silica
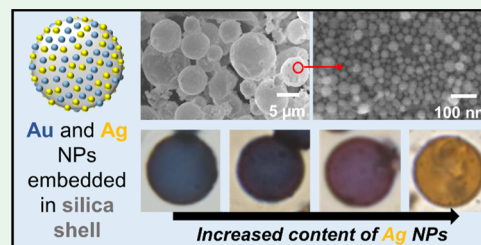
## 1. INTRODUCTION

In the last decades, inorganic, organic, and carbon-based nanoparticles (NPs) have become prominent components in the development of new technologies due to their unique physical, chemical, and biological properties.[1,2] In comparison with bulk materials, and because of their small size and larger surface area to volume ratio, NPs show enhanced properties such as reactivity, mechanical strength, sensitivity, stability, thermal conductivity, catalytic activity, light absorption, and scattering.[2,3] NPs assembled into two- or three-dimensional architectures offer new collective optical, magnetic, and electronic properties.[4,5] For instance, due to plasmon coupling, closely packed gold (Au) and silver (Ag) NPs absorb light at longer wavelengths than when they are several tenths of nanometers apart.[6–8] To fully benefit from these new collective properties, the spatial organization of the NPs often needs to be carefully controlled.[5,9,10] Such spatial organization can be obtained from the spontaneous self-assembly of NPs in solution.[5,11]

Recently, Pickering emulsions have been used as templates for the self-assembly of NPs into micron-size supracolloidal 3D structures called colloidosomes.[12,13] In the design of these structures, NPs are used as building blocks. Colloidosomes are then converted into mechanically resistant and less porous

microcapsules (MCs) by external locking steps such as particle cross-linking, macromolecules adsorption, or interfacial polymerization.[14] These MCs can be tailored to several applications and dispersed in a wide range of media while combining properties directly resulting from the details of the core (size, shape, and type of NPs) and shell (thickness, elasticity, and porosity...) (see Figure 1). Initially, the intended primary use of these new structures was the encapsulation and the controlled release of active ingredients.[13,14] With the development of preparation methods and NPs, the application range has extended to other applications in optics as strong absorbers,[15] in catalysis,[16,17] in biomedical engineering for photo acoustic imaging and photo thermal therapy,[18] and in mechanical and chemical sensing (Figure 1).[19–22]

Lately, an increasing research interest has been dedicated to the integration of several types of NPs into multifunctional colloidosomes or MCs. Despite the interest of the scientific
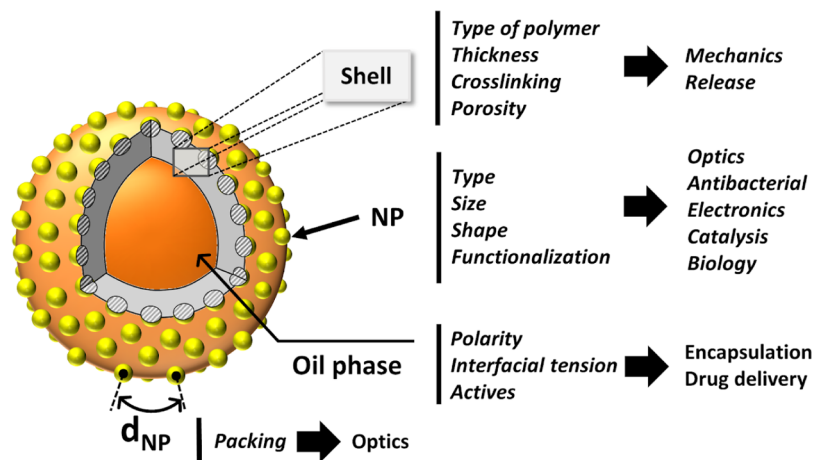
**Figure 1.** Schematic representation of the MCs' properties and applications driven by the modulation of their building blocks.

community, only few examples of this new type of supra-colloidal object have so far been reported. For instance, Bollhorst et al. reported colloidosomes with two types of NPs (superparamagnetic iron oxide and fluorescent silica) which could be useful in various biomedical applications including biosensing and bioimaging.[23,24] Additionally, Chen et al. have made permeable TiO$_2$−polystyrene hybrid hollow sphere by emulsion templating which present many applications in the field of drug release and photocatalysis.[25]

Recently, we have reported the synthesis of a novel family of multifunctional hybrid micro objects, namely, plasmonic-based mechanochromic MCs,[19] and we have demonstrated that they are excellent candidates for microsensing. These MCs made of plasmonic Au NPs and silica polymer change color under elongation and demonstrate their use as a local optical detector for sensing mechanical strain at the microscale. Though the color-change effect has already been reported, the ability to tune important features of plasmonic MC's has not yet been evidenced. In this article, we show how to improve the properties of these MCs by investigating the following: the various parameters that can impact the adsorption of NPs on oil droplets, the additional formation of the silica shells around the droplet, and the advantages afforded by using a combination of two types of NPs, which allows further tunability and color variations. This work is of importance as it widens the range of applications of these microsensors (see Figure 1).

In this article, we present a comprehensive description of the synthetic conditions that lead to MCs made of a hard silica shell, with tunable plasmonic properties. Briefly, the MCs were obtained from Pickering emulsions made of metallic NPs placed at the oil/water interface. Then, a subsequent silanization reaction locks the NPs at the interface and leads to the formation of silica MCs with NPs embedded in the silica shell (Figure 2a). We show that the pH of Au NPs impacts their adsorption on the emulsion and hence the color of the final MCs. We show that the adsorption of Au NPs at the oil/water interface takes several hours to reach a final packing of 52%. Then, we demonstrate how the thickness of the silica crust can be controlled and how it influences the mechanical robustness of the MCs. Furthermore, we show that several oils can be used for the synthesis of MCs and that the relative solubility of the silica precursor and the polarity of the oil phase can also influence the final MC properties. We also

demonstrate the synthesis of "monoflavor" and "multiflavor" MCs, with, respectively, a single component or a mixture of metallic NPs embedded in the silica shell. Finally, we demonstrate using a combination of simulations and experiments that the MC optical properties can be finely adjusted by mixing Au and Ag NPs in different ratios. Controlling the optical and mechanical characteristics of MCs used as sensors is key to significant improvement in microsensing.

## 2. EXPERIMENTAL SECTION

**2.1. Materials.** Gold(III) chloride trihydrate (HAuCl$_4$, 99.9%, Sigma-Aldrich), polyethoxyorthosilicate (PEOS, Scientific Polymer Products Inc), hydrochloric acid (HCl, ACS reagent, 37%, Sigma-Aldrich), toluene (Chromasolv Plus, 99.9%, Sigma-Aldrich), 1-butanol (ACS reagent, 99.4%, Alfa Aesar), poly (diallyldimethylam-monium-nitrate-*co*-1-vinylpyrrolidone) (PVP-DADMAN, Solvay, full structural formula available in Figure S1 of the Supporting Information), sodium hydroxide (NaOH, 50%, Sigma Aldrich), ascorbic acid (ACS reagent, 99.4%, Sigma-Aldrich), hexyl acetate (99%, Sigma-Aldrich), and hexadecane (anhydrous, 99+%, Sigma Aldrich) were obtained. Deionized water was used for all experiments.

**2.2. Au NP Synthesis.** The Au NPs were synthesized by the reduction of HAuCl$_4$ with ascorbic acid and PVP-DADMAN. A solution of $6 \times 10^{-6}$ M PVP-DADMAN and $2.5 \times 10^{-3}$ M of HAuCl$_4$ was brought to boil. Then, 12.5 mL of ascorbic acid (0.1 M) was added. The solution was protected from light by aluminum foil and stirred for 1 h at 97 °C. The Au NPs were then left to rest for 1 day to remove the largest NPs. The remainder of the dispersion was centrifuged and concentrated into a few milliliters solution.

**2.3. Ag NP Synthesis.** The Ag NPs were synthesized by the reduction of AgNO$_3$ with ascorbic acid. A solution of $6 \times 10^{-6}$ M PVP-DADMAN and $5 \times 10^{-3}$ M of ascorbic acid mixed with 0.17 mL of sodium hydroxide (0.02 M) was brought to boil. Then, 0.53 mL of AgNO$_3$ (1.2 M) was added. The solution was protected from light by aluminum foil and stirred for 1 h at 95 °C. The Ag NPs were left to rest for 1 day to remove the largest NPs. The remainder of the dispersion was centrifuged and concentrated into a 5 mL solution.

**2.4. Au NP-Silica MC Synthesis (pH ∼ 10).** PEOS (0.2 g/mL) was diluted in 1 mL of toluene. The water phase (5 mL) of the emulsion contained a solution of dispersed Au NPs ([Au$^0$] = 0.02 M), butanol (0.22 M), and ammonia (10$^{-4}$ M) to adjust pH ∼ 10. The oil and water phases were emulsified together with a Branson 3210 ultrasonic bath at 30 °C for 15 min. After 3 days, the silica shell was fully formed. The MCs were recovered, cleaned, and concentrated by simple sedimentation.

**2.5. Au NP-Silica MC Synthesis (pH ∼ 1.2).** 0.2 g of PEOS was diluted in 1 mL of toluene. The water phase (5 mL) of the emulsion contained a solution of dispersed Au NPs ([Au$^0$] = 0.02 M), butanol
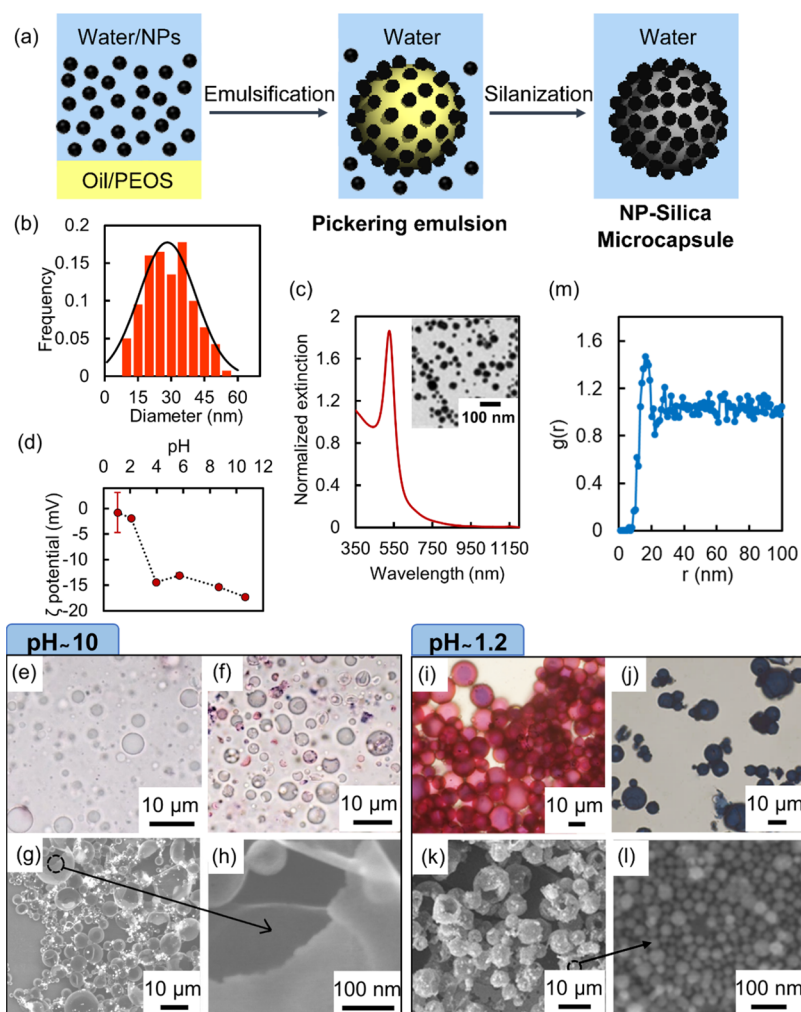
**Figure 2.** (a) Schematic representation of the NP-silica MCs' synthesis and (b) histogram of sizes of Au NPs. (c) Extinction spectrum of Au NPs normalized at 400 nm. Inset: Au NP TEM image. (d) $\zeta$ potential of Au NPs as a function of pH. (e,f) Optical microscopy images of (e) emulsion and (f) MCs and (g,h) SEM images of (g) MCs and (h) of the surface of one MC obtained with 0.02 M of Au$^0$ at pH $\sim$ 10. (i,j) Optical images of (i) Au NP-stabilized emulsion droplets and (j) MCs and (k,l) SEM images of (k) MCs and (l) the surface of one MC, evidencing the Au NPs embedded in the shell. The synthesis was performed with 0.02 M of Au$^0$ at pH $\sim$ 1.2. (m) Mean pair correlation function of the MCs with 0.02 M of Au$^0$ at pH $\sim$ 1.2.

(0.1 mL), and HCl (50−150 $\mu$L) to adjust pH to about 1.2. The oil and water phases were emulsified together (Branson 3210 ultrasonic bath) at 30 °C for 15 min. After 3 days, the silica shell was fully formed. The MCs can be recovered, cleaned, and concentrated by simple sedimentation.

**2.6. Ag NP-Silica MC Synthesis.** The protocol used was the same as the one for the Au NP-Silica MCs (pH $\sim$ 1.2). The water phase contained Ag NP at 0.6 wt % instead of Au NPs.

**2.7. Ag−Au NP-Silica MC Synthesis.** The protocol used was the same as the one for the Au NP-silica MCs (pH $\sim$ 1.2). Mixtures of Au and Ag NPs in different wt % ratios were used instead of Au NPs alone.

**2.8. Electron Microscopy.** Shape and size of the MCs were analyzed by scanning electron microscopy (SEM). SEM was performed on a JEOL 7500 HR scanning electron microscope. The samples were prepared by air-drying under ambient conditions a drop of MC dispersion on an electron microscopy carbon-coated copper grid. Environmental SEM was conducted on a FEI Quanta 600 at 1.5 Torr using water vapor. Transmission electron microscopy (TEM) was carried out on a JEOL JEM-1400 electron microscope. The accelerating voltage was set at 120 kV.

**2.9. Optical Characterization.** The color, shape, and size of the MCs were analyzed by optical microscopy. Optical microscopy images were acquired on an Olympus microscope in bright field and

transmission mode. Images were taken with a 100× objective oil of NA 1.4; no filter was used. The camera used was a Sony $\alpha$ Nex-7 color camera. The illumination power was set to a third of the intensity of a 100 W lamp and the acquisition time was 10 ms. For the image analysis, the contour of each capsule on the image was detected and the red level of the intensity on the 8 bits color camera was recorded. The red color is the average performed on a circle of size $R/2$ by $R/2$ centered in the middle of the capsule, where $R$ is the radius of the capsule. No background subtraction was performed. Optical extinction spectra were recorded in the transmission mode using a Cary 5000 spectrophotometer. Single MC extinction spectra were recorded using a CRAIC microspectrophotometer mounted on an Olympus BX51 optical microscope equipped with a 40× air objective and a 100 W halogen lamp. The spectra start at 450 nm due to the limit of detection of the microspectrophotometer used (Figure S2).

Photo images of vials were taken with a Canon PowerShot SX210IS camera (Figure S3).

**2.10. pH Measurements.** The pH of the Au NP solutions was measured with a VWR Scientific digital pH temperature meter (model 8015).

**2.11. Zetametry Measurements.** The zeta potential of the Au NPs ([Au$^0$] = 0.57 mM, [NaCl] = 10−3 M, [Ascorbic acid] = 0.054 mM) and of the Ag NPs ([Ag$^0$] = 0.005%, [NaCl] = 10−3 M,

[ascorbic acid] = 0.054 mM) as a function of the pH was measured on a Zetasizer Nano Series 200.

**2.12. Simulations.** To simulate the optical properties of NPs in silica films, we need to generate NP packing that closely resembles the local packing structures on the surface of experimental MCs. We note that we are unable to directly simulate entire MCs given their large size, so instead, flat layers resembling the local NP packings are generated. One approach to generate these simulated packings is to take experimental SEM images of NPs at the surface of MCs and to identify the perimeter of each NP. This is the first approach that was adopted, NP perimeters were manually identified, and, assuming NPs were perfectly spherical, we were able to reconstruct a packing of NPs. The packings obtained by this method are designated as "SEM packings". This method, though efficient, has one drawback: for mixtures of Au and Ag NPs, we cannot identify whether an observed NP is Au or Ag. To overcome this problem, we numerically generated packings close to the experimental ones.

To generate these packing, we used DCCP software, available at the following url: https://github.com/cvxgrp/dccp. DCCP software uses an algorithm, which minimized the total surface area occupied by a population of NPs, hence ensuring a tightly packed assembly. This can be done by entering, as an input, a set of NPs (Au and/or Ag) with each NP having a previously assigned diameter. The diameter for each NP was randomly chosen within a lognormal distribution, the parameters of which were measured using SEM images of NPs. More details are provided in the Supporting Information section (Figure S4). Such a method based on DCCP software allowed us to generate very closely packed assemblies of pure Ag or Au NPs and a mixture of both NPs. By using parameters that were measured experimentally, we could create packings that are very close to the experimental ones. These packings are designated as "DCCP packings" and are used for data shown in the last figure. We note that there is a larger potential difference between the DCCP packings and their experimental counterparts, given the larger fluctuations both in size and material type for these packings. As such, these simulations can only provide a qualitative comparison with the experimental data.

To evaluate the importance of the polydispersity of the packing, we generated similar random packing, but with a monodisperse population of NPs rather than a polydisperse population. The DCCP software is not the right tool to generate such a packing: because the algorithm is based on a minimization of the occupied area fraction, starting from a monodisperse population, it would only generate a very ordered crystalline pattern, possibly with a few defects and dislocations in the crystalline domain. Therefore, to create monodisperse packings, we used a different strategy. We distributed the monodisperse beads using a Monte Carlo simulation with a hard spheres potential to allow for a level of disorder. This potential was slightly modified with an extra term that harshly penalized touching beads to ensure that the NPs remained separate and periodic boundary conditions were also applied. Ordered monodisperse packings were generated by replacing this potential with an electrostatic potential at 0 K.

The structures were then imported into a finite difference time domain (FDTD) simulation package (Lumerical Solutions) for optical analysis. The NPs were embedded at the center of a 60 nm thick silica slab (see the Supporting Information section) and NPs larger than the layer were covered with an additional 3 nm silica coating applied to ensure that they are engulfed in silica similar to the experiments. Simulations were performed with a periodic boundary in the plane of the NPs to resemble the local MC environment, and the transmission coefficient was calculated in the normal direction (details in Supporting Information section, Figure S5). A comparison of the SEM and DCCP packing simulations can be found in Figure S6. The obtained simulated extinctions were compared with the experimental extinction of the MCs.

## 3. RESULTS AND DISCUSSION

**3.1. Adsorption of NPs.** The MC synthesis by emulsion template using Au NPs is schematized in Figure 2a. A solution

of toluene containing PEOS is emulsified in the continuous aqueous phase of the previously synthesized Au NPs. A Pickering emulsion stabilized by Au NPs is obtained.[10] The Au NPs are further locked at the oil/water interface by interfacial polycondensation of the PEOS giving rise to a silica crust embedding Au NPs.[26,27] First, Au NPs functionalized with poly(diallyldimethylammonium-nitrate-*co*-1-) vinylpyrrolidone (PVP-DADMAN), full structural formula available in Figure S1, are synthesized by the reduction of Au salt with ascorbic acid.[19,20,28,29] The precise synthetic protocol is described in details in the Experimental Section. The Au NPs obtained are polydisperse, the mean diameter is $\delta$ = 30 nm $\pm$ 11 nm and the maximum of their sharp plasmon peak is situated at $\lambda_{max} \sim 525$ nm (TEM images, histogram of size distribution, and extinction spectrum of the Au NPs can be found in Figure 2b,c). In this size range, the polydispersity does not affect the position of the plasmonic peak but results in a small broadening of this peak.[19] We have previously shown that the Au NP adsorption and packing on oil droplets require the following: (i) the right hydrophobic/hydrophilic balance of the NPs, (ii) the neutralization of the charges at the NP surface, and (iii) the use of rather large quantities of NPs.[19] It was demonstrated that condition (ii) could be met by adjusting the pH of the Au NP dispersion below 4. $\zeta$ potential results presented in Figure 2d confirm these observations. Two surface potential-dependent regimes appear with a sharp transition between pH values 2.1 and 4. For pH $\geq$ 4, the Au NP surface potential decreases to about $-15$ mV, whereas when pH $\leq$ 2.1, the Au NP surface potential increases to $-2$ mV. MCs were fabricated at two distinct pH values ($\sim$1.2 and $\sim$10) corresponding to the two surface potential regimes observed. The impact of the pH on the final MCs coverage by Au NPs is shown in Figure 2e−l. At pH $\sim$ 10, shortly after the sonication, the emulsion droplets are transparent (Figure 2e). In contrast, at pH $\sim$ 1.2, shortly after sonication, the emulsion exhibits an intense pink color (Figure 2i). The silica shell obtained by polycondensation of the PEOS at the interface is fully formed after 3 days of polymerization at room temperature.[26] The MC optical microscopy and SEM images are presented in Figure 2f−h,j,l. At pH $\sim$ 10, colorless spherical MCs without Au NPs embedded in the silica shell are observed (Figure 2f−h). At pH $\sim$ 1.2, the spherical MCs of diameter in the range of 1−15 $\mu$m present a deep blue color (Figure 2j,k) and a monolayer of densely packed gold NPs on their surface is observed (Figure 2l). At pH $\sim$ 10, the Au NPs are too negatively charged ($\zeta \sim -15$ mV) and thus cannot adsorb on the oil droplets. Therefore, no Au NPs are observed in the final MCs' silica shell. Conversely, at pH $\sim$ 1.2, the negative charges present on the Au NPs are neutralized ($\zeta \sim -2$ mV), allowing adsorption of Au NPs on the oil droplets.[19] The fabrication of MCs at pH 3.5 (intrinsic pH of the Au NPs dispersion) was also attempted. Interestingly, a pink emulsion was obtained attesting of the Au NP partial adsorption (intermediate $\zeta$ potential), but a silica layer was not formed at the o/w interface. This can be explained by the fact that an acid or base catalyst is needed to polymerize the silica precursor. The fabrication of the plasmonic MCs is an interplay between silica polycondensation and plasmonic NP adsorption at the o/w interface. Further studies would need to be performed to assess the minimum concentration of acid or base needed for interfacial silica polycondensation. The mean pair correlation function $g(r)$ of Au NPs embedded in the silica shell of the blue MCs was computed by extracting the NP center identified

on SEM images (Figure 2l). Results presented in Figure 2m reveal that the peak corresponding to the NPs first neighbors is shown around 31 nm. Because we estimate the mean radius of the Au NPs to be $15 \pm 6$ nm, we conclude that the Au NPs are close-packed, as confirmed by the SEM image shown in Figure 2l, therefore allowing for a strong plasmon coupling of the NPs.

The kinetics of adsorption of Au NPs at the oil/water interface was studied by optical microscopy. The change in color of the oil droplets as a function of time was monitored over 24 h and can be seen in Movie 1. Images (a−f) of Figure 3 present a series of snapshots from Movie 1, showing that the
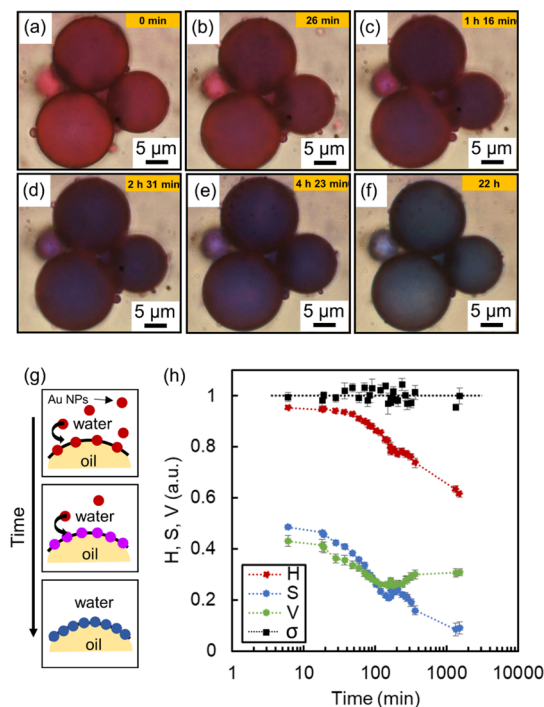


**Figure 3.** (a−f) Color change of the droplets due to the adsorption of Au NPs as a function of time. (g) Schematic representation of Au NP adsorption at the oil/water interface over time and consequent change of color of the droplets. (h) Hue, saturation, value (H, S, and V respectively—dots), and $\sigma$-radius of oil droplets normalized by the radius of oil droplets at 0 min (squares) as a function of time (values were averaged on five oil droplets).

initial pink droplets slowly turn purple within 2 h and become blue overnight. A schematic representation of the adsorption of the Au NPs at the oil/water interface and the consequent change of color of the droplets is shown in Figure 3g. The HSV color model was selected instead of the well-known RGB representation because it is closer to how human eye perceives color. This color space describes colors with the hue (H), the shade (S), and the brightness value (V). The H, S, and V values averaged over five droplets as a function of time are shown in Figure 3g. Over the course of the experiment, H decreases from 0.9 (red) to 0.6 (blue). Concomitantly both S and V decrease, proving that more light is absorbed by the MCs due to both an increase of the packing of NPs at the interface and the plasmon absorbance due to the coupling between the Au NPs. Additionally, $\sigma$ (radius of oil droplets normalized by the radius of oil droplets at 0 min) remains constant over time. This demonstrates that the color change of the droplets is due to the Au NP packing on the droplets'

surface through the NP adsorption over time rather than caused by evaporation of the solvent inside the droplets which would also lead to a decrease of the NP interparticle distance hence to a change of color.

The experimental extinctions of the blue Au MCs were obtained using a microspectrophotometer and were compared with calculated extinctions of closely packed Au MCs and loosely packed Au MCs obtained by FDTD simulations (Figure 4a). We reconstructed pure Au NP packing from SEM
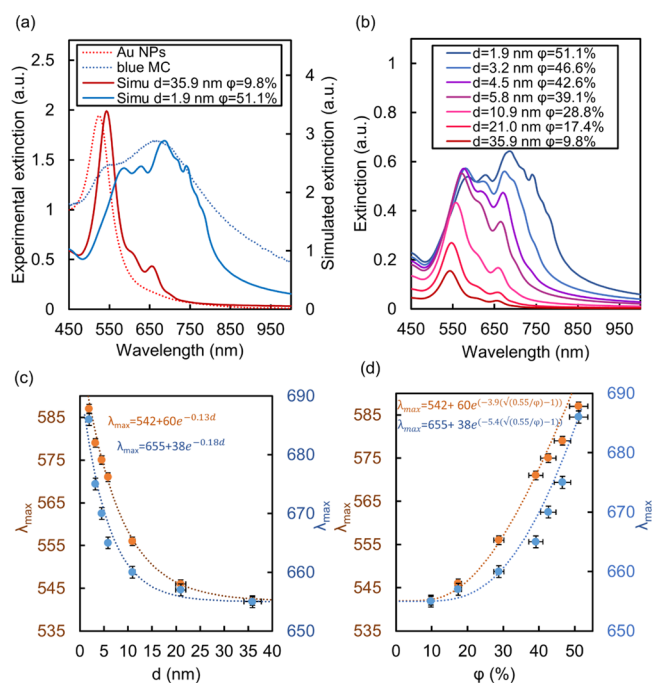


**Figure 4.** (a) Simulated and experimental optical spectra of pink emulsion and blue Au MCs. The experimental and simulated spectra are normalized at 450 nm to account for differences in Au concentrations. (b) Simulated extinction spectra of MCs with different distance between Au NPs (named "d"), and packing of Au NPs ($\varphi$). (c) Shift of the maximum of adsorption at 545 and 655 nm as a function of d. (d) Shift of the maximum of adsorption at 545 and 655 nm as a function of $\varphi$.

images and used these packings ("SEM packings") to compute the transmission and extinction $E_0$ (pure Au NP MCs) through a surface of packed NPs embedded in a silica medium. The extinction calculations were performed using FDTD simulations as detailed in the Experimental Section as well as in the Supporting Information section. We use the notation "d" for the mean separation distance between NPs (distance surface to surface). A good agreement between the spectral features of experimental and simulated extinctions was obtained for d = 1.9 nm and $\varphi$ = 51% volume fraction in the case of the blue MCs and for d = 35.9 nm and $\varphi$ = 9.8% in the case of the loosely packed Au MCs (based on other experiments not shown here, these MCs are pink). For the simulated pink MCs, a sharp plasmon peak was observed at 542 nm corresponding to the extinction peak of well-dispersed Au NPs ($\lambda_{max} \sim 525$ nm) red-shifted due to the presence of the silica and toluene. For the experimental blue MCs, a wide plasmon band around 700 nm was observed and a small plasmon shoulder around 535 nm corresponding to the peak of dispersed Au NPs (see Figure S2 for more blue MCs optical spectra). The simulated extinctions of the MCs as a function of the distance between

the Au NPs are reported in Figure 4b. As the distance between the Au NPs decreases, the intensity of the plasmon peak of uncoupled Au NPs (530 nm) decreases, while the wide plasmon band characteristic of coupled Au NPs is red-shifted and its intensity increases. The maximum of the plasmon peaks around 542 and 655 nm as a function of the mean separation distance between Au NPs ("d") are shown in Figure 4c. Both shifts can be reasonably fit to an exponential decay function with a decay length ($d^*$) of about 6−8 nm, which is approximately about 20−25% of the Au NP mean diameter. This is consistent with previous data reported in the literature for single pairs of NPs.[28] The maximum of the plasmon peaks around 542 and 655 nm as a function of the packing of Au NPs ($\varphi$) are shown in Figure 4d. Interestingly, we found that we can extend the principle of the "ruler equation" described by Jain et al.[30] derived for two isolated NPs to the case of NP packings. Using the scaling derived by Hoffman and Kevelam,[31] we can relate the mean separation distance between NPs ("d") to the area fraction $\varphi$. In a two-dimensional system

$$d = 2r \left( \sqrt{\frac{\phi_m}{\phi}} - 1 \right)$$

where $r$ is the AuNPs' mean radius (15 nm) and $\varphi_m$ is the maximum area fraction of a polydisperse packing. We find that by adjusting $\varphi_m$ to 0.55 and replacing d in the "ruler" equation by the above equation, we can fit with accuracy the position of the plasmonic peaks when it is plotted versus the area fraction $\varphi$. This shows that the characteristic $d^*$ extracted from the "ruler" equation equates the mean distance between the AuNPs in a random packing. It is important to emphasize the fact that with the same $\varphi_m$, the curves for both peaks are well adjusted. This result shows that it is possible to predict the positions of plasmonic peaks when the packing fraction is changed.

**3.2. Morphology of the Silica Shell.** The brittleness of the MCs has a significant impact on the mechanical and therefore on the final optical output of the MCs used as sensors. A shell more brittle leading to sensing of more minute mechanical deformations for instance. The impact of the concentration of PEOS ([PEOS]) on the thickness of the shell and on the mechanical robustness of the MCs is presented in Figure 5. Based on the SEM images of the crust shown in Figure 5a−e and the graph in Figure 5f showing the thickness of the shell as a function of [PEOS], one can see that the thickness of the crust increases with the increase of [PEOS]. Three distinct areas are identified in Figure 5f. These areas correspond to the formation of spherical capsules, "hemi-capsules" and totally buckled capsules. Each area is delimited by [PEOS] and the corresponding shell thickness. At low [PEOS] (∼0.05 g/mL), the shell formed is very thin (Figure 5a shows a translucent shell hard to image) and the MCs totally collapse upon drying, as shown in Figure 5g. For [PEOS] = 0.1 g/mL, the thickness of the shell increases up to about 40 nm and the dried MCs buckle into "hemispheres". The "top half "of the shell fell inside the "bottom half" of the shell (see Figure 5g). Upon the increase of [PEOS] (0.2 g/mL), the formed silica shell is thicker (about 61 nm, Figure 5c,g). At these concentrations, the MCs retain their spherical shape upon drying, as shown in Figure 5g. For [PEOS] ∼ 0.2 g/mL, the obtained MCs remain spherical upon drying (see Figure 5g). The silica shell becomes thicker for 0.3 and 0.4 g/
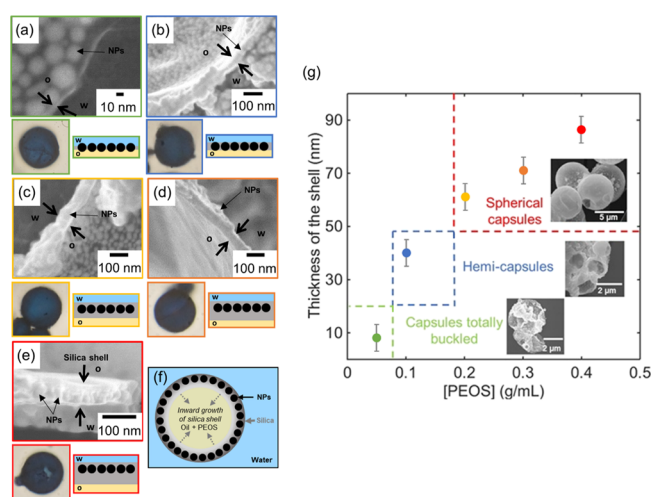


**Figure 5.** (a−e) SEM images of the shell of the Au−Si MCs obtained with (a) 0.05, (b) 0.1, (c) 0.2, (d) 0.3, and (e) 0.4 g/mL PEOS. The oil phase "o" is toluene and the aqueous phase "w" is water. The black arrows indicate the localization of the Au NPs within the silica shell. The single blue MCs are about 10 μm. (f) Schematic representation of the growth of the silica shell embedding the NPs. (g) Au−Si MC shell thickness and buckling as a function of the concentration of PEOS (g/mL).

mL of PEOS (Figure 5d−g). The thickness of the silica shell had very little to no impact on the optical properties of the MCs. Indeed, the MCs with different shell thickness have similar blue color to the naked eye (Figure 5a−e) and the simulated extinction of Au NPs tightly packed within silica layers of different thicknesses overlap (Figure S7). The results presented here are consistent for MCs of diameter ≤10 μm which constitutes the majority of the samples observed. For the few capsules of diameter above 10 μm, 0.2 g/mL PEOS was not enough to avoid buckling, which suggests that not only the thickness of the silica shell matters but also the ratio between the size of the MCs and the shell thickness is an important parameter to consider.

So far, we have demonstrated the successful synthesis of MCs with toluene;[19] it is therefore questionable whether this approach can be generalized to other organic solvents. The fabrication process of MCs was extended to hydrophobic oils of different polarities. While keeping the exact same formulation ([Au⁰] = 0.02 M, [butanol] = 0.22 M, [PEOS] = 0.2 g/mL, pH ∼ 1.2), toluene slightly soluble in water was first replaced by a very hydrophobic oil insoluble in water and non-polar (hexadecane) and then by a mixture of hexadecane/hexyl acetate (50/50 by volume) to increase the oil polarity of the oil phase. The MCs obtained using hexadecane and hexadecane/hexyl acetate are shown in Figure 6a,c,d,f and are compared to the ones obtained with toluene (Figure 6b,e). Simulations presented in Figure S8 show that changing the oil has very little impact on the extinction of the MCs. This is most likely due to two factors: (i) the three oils studied have a close refractive index and (ii) the formation of a silica shell for the three oils studied. All the MCs obtained are blue (Figure 6a−c) due to the closely packed Au NPs embedded in their shells (see insets of Figure 6d,f). In the case of hexadecane, which is the least polar solvent, numerous broken MCs can be seen in Figure 6a. Upon increase of the polarity using either toluene or hexadecane/hexyl acetate mixture, the MCs obtained are undamaged (Figure 7b,c). The observed lack of
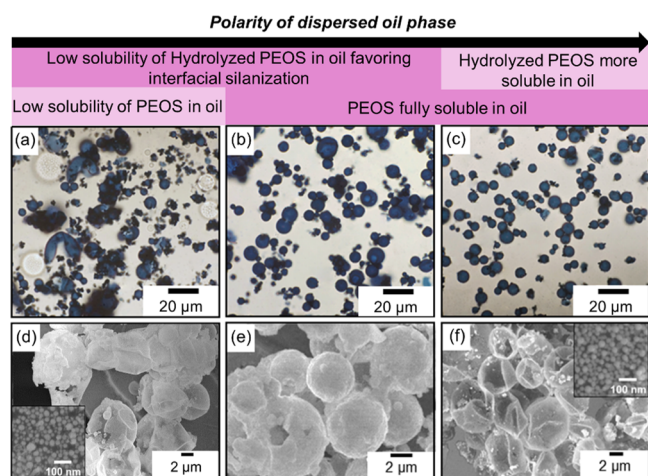
**Figure 6.** (a−c) Optical images of Au−Si MCs obtained with (a) hexadecane, (b) toluene, and (c) hexadecane/hexyl acetate 50/50 v/v. (d−f) SEM images of Au−Si MCs obtained with (d) hexadecane, (e) toluene, and (f) hexadecane/hexyl acetate 50/50 v/v. Insets show the surface of a typical MC for (d) hexadecane and (f) hexadecane/hexyl acetate 50/50 V/V. All syntheses are carried out with 0.2 g of PEOS.

solubility of PEOS in the least polar solvent, here hexadecane (hazy mixture, see Figure S3a), limits the formation of a robust silica shell at the oil/water interface for larger MCs and actually leads to the formation of silica particle (see Figure S3b). Upon increase of the oil polarity, PEOS becomes fully miscible in the oil and permits the formation of the silica shell at the oil/water interface. The polarity of the oil also influences the solubility of PEOS hydrolyzed under acidic conditions. Due to its increased polarity, hydrolyzed PEOS is more soluble in polar solvent. Thus, hydrolyzed PEOS is poorly soluble in hexadecane alone. In the presence of hexyl acetate, hydrolyzed PEOS can desorb from the interface due to its increased solubility in the oil phase, rendering the interfacial polycondensation more difficult (less robust shell buckle upon drying, Figure 6f). The polarity of toluene is between the polarity of hexadecane and the one of the hexadecane/hexyl acetate mixture. Thus, with toluene, PEOS is fully soluble in the oil phase and hydrolyzed PEOS is "locked" at the oil/water interface, therefore favoring the interfacial polycondensation and the formation of a robust MC shell. A noticeable thicker silica shell can be observed with toluene in Figure 6e as compared to the two other solvents/solvent mixture (Figure 6d,f). From the presented data, we can conclude that the morphology of MCs templated by o/w Pickering emulsions is a delicate interplay between the Au NP adsorption, oil polarity, and silica precursor solubility and concentration.

**3.3. "Multiflavor" MCs.** So far, only synthesis of MCs with one kind of NPs embedded in the silica crust has been reported.[19] This synthesis fact limits our ability to tune the optical characteristics of MCs used as optical microsensors. To allow such a tunability, the NP-silica MC synthetic method is extended to different types of NPs and mixture of NPs to create the so-called "multiflavor" MCs. Ag NPs are synthesized by following a similar protocol to that used to synthesize Au NPs (see the Experimental Section). The obtained Ag NPs are polydispersed, as shown by the TEM image and the histogram of the distribution of sizes (Figure 7a). The mean diameter of the Ag NPs is around $33 \pm 13$ nm. Ag NPs exhibit a sharp plasmon absorption ($\lambda_{max} \sim 417$ nm) and a yellow color from
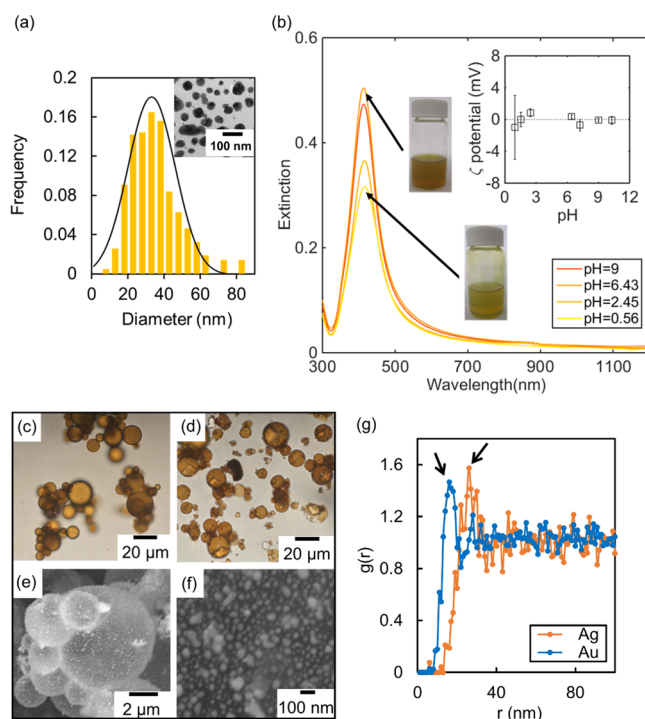


**Figure 7.** (a) Histogram of sizes of Ag NPs. Inset: TEM image of Ag NPs. (b) Extinction of Ag NPs as a function of pH. The two pictures, respectively, show the dispersed solution of Ag NPs of the same concentration at pH = 9 and pH = 0.56. Inset: zeta potential of the Ag NPs as a function of the pH. (c,d) Optical images of (c) Ag NP-stabilized emulsion droplets and (d) Ag MCs and (e,f) SEM images of (e) Ag MCs and (f) the surface of one Ag MC, evidencing the Ag NPs embedded in said shell. The synthesis was performed with 0.6% of Ag at pH 1.2. (g) Mean pair correlation function for MCs made of Ag NPs compared to the ones made of Au NPs.

pH 0.6 to pH 9, as shown in Figure 7b. Zetametry experiments show that Ag NPs are very weakly charged ($\zeta$ potential ∼0 mV) and remain well dispersed in water at pH ranging from 1 to 11. These observations suggest that unlike the Au NPs, the Ag NPs are not stabilized by electrostatic charges coming from ascorbic acid adsorbed at the NP surface but are instead primarily sterically stabilized by the PVP-DADMAN. This result is consistent with the previous literature referencing that PVP interacts, adsorbs, and strongly stabilize Ag NPs.[32] Silver−silica MCs are synthesized with Ag NPs embedded in the silica crust by following the same emulsion template process as the one used for Au MCs. Toluene was chosen as the oily phase. We observe that Ag NPs adsorb at the interface oil/water at any pH, which is consistent with the fact that Ag NPs have a very low surface charge, which does not depend on pH (Figure 7b). Because pH also affects the polycondensation of silica precursor, to remain consistent with the previous shell formed, the Ag−Si, MCs are synthesized at the same pH as the one set for the synthesis of Au MCs (pH ∼ 1.2). The obtained Pickering emulsion imaged in Figure 7c has a yellow color. Once condensation of the PEOS at the oil/water interface has occurred, yellow Ag MCs are obtained (Figure 7d). SEM images in Figure 8e,f show the typical aspect of the Ag MCs and the Ag NPs embedded in the silica shell, respectively. The mean pair correlation function g(r) for Ag NPs within the silica shell of the Ag MCs was computed by extracting the NP center identified on SEM images (Figure 7f). Results compared to the previously discussed g(r) of Au NPs in MCs are presented in
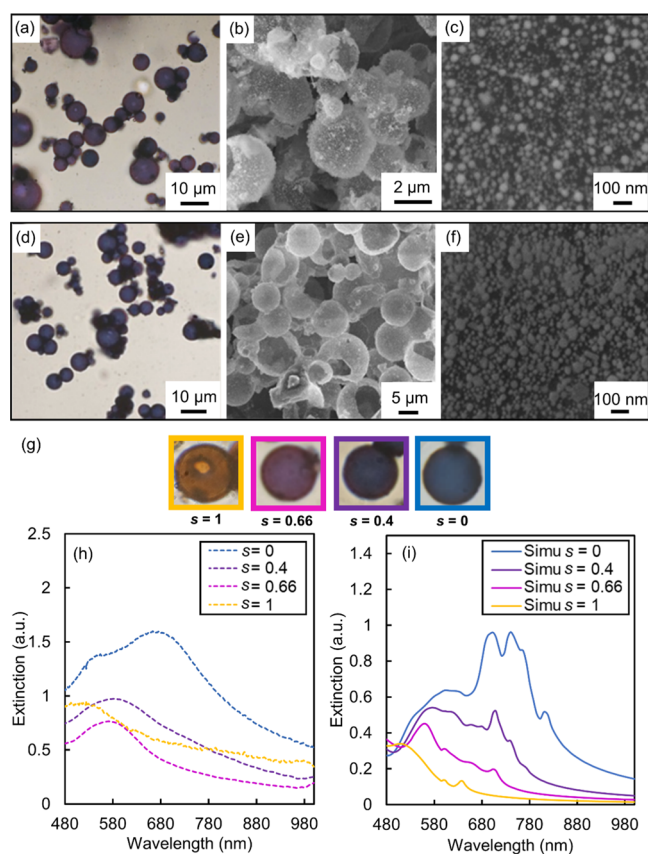
**Figure 8.** (a−f) Mixtures of Au and Ag NPs were used to form multiflavored MCs. (a) Optical images and (b,c) SEM images of MCs and MC surface made with s = 0.4. (d) optical images and (e,f) SEM images of MCs and MC surface made with s = 0.66. (g) MCs at s = 1, s = 0.66, s = 0.4, and s = 0 with $s = N_{Ag}/(N_{Ag} + N_{Au})$. (h) Experimental and (i) simulated extinction spectra of the plasmonic MCs for s = 0, d = 2.8 nm, and $\varphi$ = 52.6%; for s = 0.4, d = 5.8 nm, and $\varphi$ = 39.7%; for s = 0.66, d = 9.0 nm, and $\varphi$ = 34.9%; and for s = 1, d = 15.6 nm, and $\varphi$ = 25.0%.

Figure 7g. For Ag MCs, the first neighbor peak is located at 49 nm. The Ag NPs mean radius being 16 ± 7 nm; on average, the distance between the surfaces of the Ag NPs is about 17 nm. This is in contrast with the almost touching Au NPs in the Au MCs, leading to strong plasmon coupling (Figure S9b). We believe that the separation is due to the strong PVP-DADMAN adsorption on Ag NPs. Under such surface separation conditions, plasmons cannot strongly couple, which is consistent with the fact that Ag MCs always appear yellow (Figure S10b).

MCs containing Au and Ag NP mixtures at two different ratios s = 0.4 and 0.66 by number of NPs for Au and Ag, respectively, $s = N_{Ag}/(N_{Ag} + N_{Au})]$ were prepared. The protocol is similar to that used for the synthesis of Au MCs except for the initial aqueous solution, which is a mixture of Au and Ag NPs suspended in solution. For both ratios s, spherical silica MCs with closely packed NPs embedded in a silica shell were obtained (see Figure 8a−f below and Figure S11 for EDS images, showing both Au and Ag NPs on the MCs surface). Depending on s, MCs of different colors are obtained. At s = 0.4, the MCs are light purple (Figure 8a), whereas at s = 0.66, they are dark purple (Figure 8d). The experimental extinction spectra of single MCs obtained using a microspectrophotometer are compared with simulated extinction spectra of the

DCCP packings and presented in Figure 8g−i (see details in the Experimental Section). Overall, a good agreement between the experimental (Figure 8h) and simulated (Figure 8i) spectra are observed. For pure Au NPs, the extinction curves shows very wide extinction peaks around 700 nm likely resulting from the superposition of peaks due to the distribution of surface to surface separation in a random packing. The second peak (or shoulder) of absorption is visible at around 525 nm: it corresponds to the regular absorption peak of uncoupled NPs embedded in silica as detailed previously.[33] This peak becomes more and more dominant over the coupled Au NPs peak as the amount of Ag is increased. Differences between experimental and simulated extinction curves can be explained by the fact that microspectrometry allows us to measure the optical properties on a scale of the order of about 10 μm, whereas simulations provide optical properties on a scale of about 300 nm. As such, simulated packings lack heterogeneities in particle size and interparticle distance. Moreover, simulations do not capture the pathway of light through the inside of the MCs.

Our simulations using the DCCP packings (Figures 8i, S9, and S10) reveal that for both Au and Ag NPs, a plasmon redshift is caused by (i) the number, position, and type of the NP neighbors; (ii) the plasmon coupling between close NP neighbors and in much larger effect by (iii) the presence of toluene inside the MCs or the silica shell embedding the NPs.[30,34−37] This is because the refractive indexes of toluene (1.5) and silica (1.46) are higher than the refractive index of pure water (1.33), resulting in stronger inter-NP coupling.[35,38,39]

As Au NPs are diluted with Ag NPs in the packing, we can observe an overall shift toward smaller wavelength of the main extinction peak (∼700 nm). These facts suggest that for these mixture cases, absorption results from both Ag NP noncoupled plasmons and coupled plasmons of Au NPs on the surface. To verify this hypothesis, we have separately "removed" Ag and Au NPs from Au Ag NP packings and compared the resulting extinctions to the one of the mixture of NPs (Figure S12). Results showed that Ag NP plasmons are not coupled or are coupled to only a small extent. For pure Ag MCs, a broad peak with a maximum of absorption situated at 520 nm is observed likely resulting from the superposition of peaks due to the distribution of surface-to-surface separation in a random packing. In pure Ag MCs, Ag NP plasmons remain for the most part uncoupled.

Our experimental data for coupled NPs on MCs gave broad extinction peaks. Interestingly, our simulations (Figure S13) indicate that the optical response of disordered packings of monodisperse Au NPs in MC would likely not be significantly different from the extinction observed experimentally with disordered packings of polydisperse Au NPs. Furthermore, additional simulations show that the extinction band of disordered packings of polydisperse Au NPs can be further red-shifted as compared to the extinction band of ordered packings of monodisperse Au NPs[40−42] because a smaller average interparticle distance can be obtained with polydispersed Au NPs as compared to monodisperse Au NPs (Figure S14).[43]

## 4. CONCLUSIONS

In this work, we have presented a simple and versatile approach for the tailored design of plasmonic silica MCs based on the self-assembly of NPs. The MCs were fabricated using o/w Pickering emulsions as templates in combination with a

silica precursor PEOS as an interfacial binder for plasmonic NPs. The pH of the NP dispersion, the solubility and concentration of PEOS in the oil phase, as well as the type of NPs are as many parameters that control the mechanical and optical properties of the final MCs. At very acidic pH, Au NPs closely pack at the emulsion interface, the plasmons of Au NPs couple leading to blue MCs. On the contrary, the plasmons of "loosely" packed Ag NPs do not couple, leading to yellow MCs. Spherical MCs resistant to air-drying were obtained with [PEOS] > 0.2 g/mL well solubilized in a polar oil such as toluene. Mono- or multiflavored MCs of different colors from yellow to blue were obtained by mixing Au and Ag NPs in different ratios. The simulated plasmonic response of all the different MCs were in close agreement with the experimental results, thus validating our approach. Further simulation findings revealed that the refractive index of the inner oil phase and of the MCs shell have a large impact on the plasmonic response and hence on the color of the MCs. Our emulsion template technique opens new gateways for the design of multifunctional MCs with properties arising from the individual or the combination of the properties of each one of its building blocks. Among other, we have shown that the MCs can be used for strain microsensing.[19] The use of several types of NPs in the crust and the control of the silica shell thickness are gateways toward a finer control of the optical character-istics of MCs used as optical microsensors. Such versatile MCs could also be applied in catalysis for the degradation of dyes, in biology using antimicrobial properties of Ag NPs, and in medicine with the encapsulation of drugs. Due to the brittleness of the shell, one can easily imagine the oil-loaded silica MCs to be considered as promising controlled release systems, where the oil soluble actives are released under mechanical force, while the plasmonic NPs can serve as an optical tracker to localize the MCs within complex matrices. We envision that MCs may be deployed as glucose sensors.[44,45] Indeed, under aerobic conditions, in the presence of glucose oxidase, glucose is oxidized. As a result of this oxidation, $H_2O_2$ is produced which, in-turn, oxidizes Ag to $Ag^+$. Over time, the degradation of Ag NPs would produce a change in the optical response of Au—Ag NP MCs. In this application, the plasmonic multiflavored MCs would translate a chemical input into a clear optical output. Other examples of potential applications include the use of capsules for the detection of species in solution, which could adsorb to NPs and change the overall optical response of the MCs.

## ■ ASSOCIATED CONTENT

### ⓢ Supporting Information

The Supporting Information is available free of charge at https://pubs.acs.org/doi/10.1021/acsanm.1c04542.

Chemical structure of PVP-DADMAN, extinction of blue Au Si MCs of different sizes, mixture of PEOS with different solvents, SEM image of Au MCs obtained with 0.2 g of PEOS in hexadecane, more details on optical simulations, impact of the silica shell thickness on the MC's extinction, impact of different oils on the MC's extinction, simulated extinction of Au and Ag NPs in different case scenarios, EDS images that illustrate the co-existence of Au and Ag NPs on the surface of the MCs, study of independent plasmon coupling of Au and Ag NPs, simulated extinctions of three disordered packings of monodisperse Au NPs, and simulated

extinctions of three organized packings of monodisperse Au NPs (PDF).

Adsorption of Au NPs on toluene droplets (AVI)

## ■ AUTHOR INFORMATION

### Corresponding Author

**Rémi Dreyfus** — *Complex Assemblies of Soft Matter Laboratory (COMPASS), UMI 3254, CNRS-Solvay-University of Pennsylvania, CRTB, Bristol, Pennsylvania 19007, United States; Laboratoire Nanotechnologies Nanosystèmes (LN2), CNRS—Université de Sherbrooke, Sherbrooke, Quebec J1K 0A5, Canada;*
Email: remi.dreyfus@cnrs.fr

### Authors

**Céline Burel** — *Complex Assemblies of Soft Matter Laboratory (COMPASS), UMI 3254, CNRS-Solvay-University of Pennsylvania, CRTB, Bristol, Pennsylvania 19007, United States;* ⓞ orcid.org/0000-0002-9645-5039

**Omar Ibrahim** — *Department of Chemistry, University of Pennsylvania, Philadelphia, Pennsylvania 19104, United States;* ⓞ orcid.org/0000-0003-2077-8613

**Emanuele Marino** — *Department of Chemistry, University of Pennsylvania, Philadelphia, Pennsylvania 19104, United States*

**Harshit Bharti** — *Department of Materials Science and Engineering, University of Pennsylvania, Philadelphia, Pennsylvania 19104, United States*

**Christopher B. Murray** — *Department of Chemistry, University of Pennsylvania, Philadelphia, Pennsylvania 19104, United States; Department of Materials Science and Engineering, University of Pennsylvania, Philadelphia, Pennsylvania 19104, United States*

**Bertrand Donnio** — *Institut de Physique et Chimie des Matériaux de Strasbourg (IPCMS), UMR 7504, CNRS-Université de Strasbourg, 67034 Strasbourg, France;* ⓞ orcid.org/0000-0001-5907-7705

**Zahra Fakhraai** — *Department of Chemistry, University of Pennsylvania, Philadelphia, Pennsylvania 19104, United States;* ⓞ orcid.org/0000-0002-0597-9882

Complete contact information is available at:
https://pubs.acs.org/10.1021/acsanm.1c04542

### Author Contributions

The manuscript was written through contributions of all authors. All authors have given approval to the final version of the manuscript. C.B. designed and performed experiments, analyzed data, and wrote the manuscript. R.D. initiated the project, analyzed data, and wrote the manuscript. H.B., E.M., and C.B.M. performed part of the micro spectrophotometry measurements and analyzed data. B.D. analyzed data and wrote the manuscript. O.I. and Z.F. performed the optical simulations, analyzed data, and wrote the manuscript.

### Funding

## ■ REFERENCES

(1) Ealias, S. A. M.; Saravanakumar, M. P. A Review on the Classification , Characterisation , Synthesis of Nanoparticles and Their Application. *IOP Conf. Ser.: Mater. Sci. Eng.* **2017**, *263*, 32019.

(2) Heiligtag, F. J.; Niederberger, M. The Fascinating World of Nanoparticle Research. *Mater. Today* **2013**, *16*, 262−271.

(3) Daniel, M.-C.; Astruc, D. Gold Nanoparticles: Assembly, Supramolecular Chemistry , Quantum-Size-Related Properties , and Applications toward Biology, Catalysis , and Nanotechnology. *Chem. Rev.* **2004**, *104*, 293−346.

(4) Podsiadlo, P.; Krylova, G. V.; Demortière, A.; Shevchenko, E. V. Multicomponent Periodic Nanoparticle Superlattices. *J. Nanoparticle Res.* **2011**, *13*, 15−32.

(5) Boles, M. A.; Engel, M.; Talapin, D. V. Self-Assembly of Colloidal Nanocrystals : From Intricate Structures to Functional Materials. *Chem. Rev.* **2016**, *116*, 11220−11289.

(6) Myroshnychenko, V.; Rodríguez-Fernández, J.; Pastoriza-Santos, I.; Funston, A. M.; Novo, C.; Mulvaney, P.; Liz-Marzán, L. M.; García de Abajo, F. J. Modelling the Optical Response of Gold Nanoparticles. *Chem. Soc. Rev.* **2008**, *37*, 1792−1805.

(7) Chen, J.; Feng, J.; Li, Z.; Xu, P.; Wang, X.; Yin, W.; Wang, M.; Ge, X.; Yin, Y. Space-Confined Seeded Growth of Black Silver Nanostructures for Solar Steam Generation. *Nano Lett.* **2019**, *19*, 400−407.

(8) Feng, J.; Xu, D.; Yang, F.; Chen, J.; Wu, C.; Yin, Y. Surface Engineering and Controlled Ripening for Seed-Mediated Growth of Au Islands on Au Nanocrystals. *Angew. Chem., Int. Ed.* **2021**, *60*, 16958−16964.

(9) Si, K. J.; Chen, Y.; Shi, Q.; Cheng, W. Nanoparticle Superlattices : The Roles of Soft Ligands. *Adv. Sci.* **2018**, *5*, 1700179.

(10) Sperling, R. A.; Parak, W. J. Surface Modification, Functionalization and Bioconjugation of Colloidal Inorganic Nanoparticles. *Philos. Trans. R. Soc. London* **2010**, *368*, 1333−1383.

(11) Yi, C.; Yang, Y.; Liu, B.; He, J.; Nie, Z. Polymer-Guided Assembly of Inorganic Nanoparticles. *Chem. Soc. Rev.* **2020**, *49*, 465−508.

(12) Pickering, S. U. Emulsions. *J. Chem. Soc. Trans.* **1907**, *91*, 2001−2021.

(13) Dinsmore, A. D.; Hsu, M. F.; Nikolaides, M. G.; Marquez, M.; Bausch, A. R.; Weitz, D. A. Colloidosomes: Selectively Permeable Capsules Composed of Colloidal Particles. *Science* **2002**, *298*, 1006−1009.

(14) Thompson, K. L.; Williams, M.; Armes, S. P. Colloidosomes : Synthesis , Properties and Applications. *J. Colloid Interface Sci.* **2015**, *447*, 217−228.

(15) Liu, D.; Zhou, F.; Li, C.; Zhang, T.; Zhang, H.; Cai, W.; Li, Y. Black Gold : Plasmonic Colloidosomes with Broadband Absorption Self-Assembled from Monodispersed Gold Nanospheres by Using a Reverse Emulsion System. *Angew. Chem., Int. Ed.* **2015**, *54*, 9596−9600.

(16) Jeong, Y.; Patra, D.; Sanyal, A.; Rotello, V. M. Fabrication of Stable Nanoparticle-Based Colloidal Microcapsules. *Curr. Org. Chem.* **2013**, *17*, 49−57.

(17) Zhang, C.; Hu, C.; Zhao, Y.; Möller, M.; Yan, K.; Zhu, X. Encapsulation of Laccase in Silica Colloidosomes for Catalysis in Organic Media. *Langmuir* **2013**, *29*, 15457−15462.

(18) Huang, P.; Lin, J.; Li, W.; Rong, P.; Wang, Z.; Wang, S.; Wang, X.; Sun, X.; Aronova, M.; Niu, G.; Leapman, R. D.; Nie, Z.; Chen, X. Biodegradable Gold Nanovesicles with Ultra-Strong Plasmonic Coupling Effect for Photoacoustic Imaging and Photothermal Therapy. *Angew. Chem., Int. Ed.* **2013**, *52*, 13958−13964.

(19) Burel, C. A. S.; Alsayed, A.; Malassis, L.; Murray, C. B.; Donnio, B.; Dreyfus, R. Plasmonic-Based Mechanochromic Microcapsules as Strain Sensors. *Small* **2017**, *13*, 1701925.

(20) Burel, C.; Teolis, A.; Alsayed, A.; Murray, C. B.; Donnio, B.; Dreyfus, R. Plasmonic Elastic Capsules as Colorimetric Reversible pH-Microsensors. *Small* **2020**, *16*, 1903897.

(21) Phan-quang, G. C.; Lee, H. K.; Phang, I. Y.; Ling, X. Y. Plasmonic Colloidosomes as Three-Dimensional SERS Platforms with Enhanced Surface Area for Multiphase Sub-Microliter Toxin Sensing. *Angew. Chem., Int. Ed.* **2015**, *54*, 9691−9695.

(22) Turek, V. A.; Francescato, Y.; Cadinu, P.; Crick, C. R.; Elliott, L.; Chen, Y.; Urland, V.; Ivanov, A. P.; Velleman, L.; Hong, M.; Vilar, R.; Maier, S. A.; Giannini, V.; Edel, J. B. Self-Assembled Spherical Supercluster Metamaterials from Nanoscale Building Blocks. *ACS Photonics* **2016**, *3*, 35−42.

(23) Bollhorst, T.; Shahabi, S.; Wörz, K.; Petters, C.; Dringen, R.; Maas, M.; Rezwan, K. Bifunctional Submicron Colloidosomes Coassembled from Fluorescent and Superparamagnetic Nanoparticles. *Angew. Chem., Int. Ed.* **2015**, *54*, 118−123.

(24) Wu, J.; Ma, G.-H. Recent Studies of Pickering Emulsions: Particles Make the Difference. *Small* **2016**, *12*, 4633−4648.

(25) Chen, T.; Colver, P. J.; Bon, S. A. F. Organic − Inorganic Hybrid Hollow Spheres Prepared from TiO 2 -Stabilized Pickering Emulsion Polymerization. *Adv. Mater.* **2007**, *19*, 2286−2289.

(26) Wang, H.; Zhu, X.; Tsarkova, L.; Pich, A.; Möller, M. All-Silica Colloidosomes with a Particle-Bilayer Shell. *ACS Nano* **2011**, *5*, 3937−3942.

(27) Zhao, Y.; Li, Y.; Demco, D. E.; Zhu, X.; Möller, M. Microencapsulation of Hydrophobic Liquids in Closed All-Silica Colloidosomes. *Langmuir* **2014**, *30*, 4253−4261.

(28) Zhang, J.; Liu, H.; Wang, Z.; Ming, N. Shape-Selective Synthesis of Gold Nanoparticles with Controlled Sizes, Shapes, and Plasmon Resonances. *Adv. Funct. Mater.* **2007**, *17*, 3295−3303.

(29) Malassis, L.; Dreyfus, R.; Murphy, R. J.; Hough, L. A.; Donnio, B.; Murray, C. B. One-Step Green Synthesis of Gold and Silver Nanoparticles with Ascorbic Acid and Their Versatile Surface Post-Functionalization. *RSC Adv.* **2016**, *6*, 33092−33100.

(30) Jain, P. K.; Huang, W.; El-sayed, M. A. On the Universal Scaling Behavior of the Distance Decay of Plasmon Coupling in Metal Nanoparticle Pairs: A Plasmon Ruler Equation. *Nano Lett.* **2007**, *7*, 2080−2088.

(31) Hoffmann, A. C.; Kevelam, J. Model for the interparticle surface separation in concentrated mono- and polydisperse suspensions. *AIChE J.* **1999**, *45*, 285−290.

(32) Wiley, B.; Sun, Y.; Xia, Y. Synthesis of Silver Nanostructures with Controlled Shapes and Properties. *Acc. Chem. Res.* **2007**, *40*, 1067−1076.

(33) Zámbó, D.; Deák, A. Optical Simulations of Self-Assembly Relevant Gold Aggregates : A Comparative Study. *Period. Polytech., Chem. Eng.* **2016**, *60*, 244.

(34) Jiang, M.-M.; Chen, H.-Y.; Li, B.-H.; Liu, K.-W.; Shan, C.-X.; Shen, D.-Z. Hybrid Quadrupolar Resonances Stimulated at Short Wavelengths Using Coupled Plasmonic Silver Nanoparticle Aggregation. *J. Mater. Chem. C* **2014**, *2*, 56−63.

(35) Shanthil, M.; Thomas, R.; Swathi, R. S.; Thomas, K. G. Ag@ SiO2 Core−Shell Nanostructures: Distance-Dependent Plasmon Coupling and SERS Investigation. *J. Phys. Chem. Lett.* **2012**, *3*, 1459−1464.

(36) Ghosh, S. K.; Pal, T. Interparticle Coupling Effect on the Surface Plasmon Resonance of Gold Nanoparticles: From Theory to Applications. *Chem. Rev.* **2007**, *107*, 4797−4862.

(37) Sheikholeslami, S.; Jun, Y. W.; Jain, P. K.; Alivisatos, A. P. Coupling of Optical Resonances in a Compositionally Asymmetric Plasmonic Nanoparticle Dimer. *Nano Lett.* **2010**, *10*, 2655−2660.

(38) Rodríguez-Fernández, J.; Pastoriza-Santos, I.; Pérez-Juste, J.; García de Abajo, F. J.; Liz-Marzán, L. M. The Effect of Silica Coating on the Optical Response of Sub-Micrometer Gold Spheres. *J. Phys. Chem. C* **2007**, *111*, 13361−13366.

(39) Mock, J. J.; Smith, D. R.; Schultz, S. Local Refractive Index Dependence of Plasmon Resonance Spectra from Individual Nanoparticles. *Nano Lett.* **2003**, *3*, 485−491.

(40) Qin, Y.; Ji, X.; Jing, J.; Liu, H.; Wu, H.; Yang, W. Size Control over Spherical Silver Nanoparticles by Ascorbic Acid Reduction. *Colloids Surf., A* **2010**, *372*, 172−176.
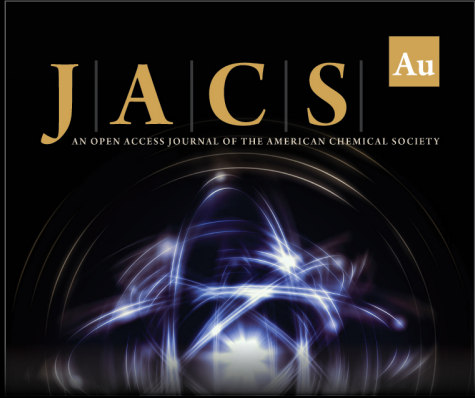
(41) Bastús, N. G.; Comenge, J.; Puntes, V. Kinetically Controlled Seeded Growth Synthesis of Citrate-Stabilized Gold Nanoparticles of up to 200 Nm: Size Focusing versus Ostwald Ripening. *Langmuir* **2011**, *27*, 11098−11105.

(42) Rodríguez-Fernández, J.; Pérez-Juste, J.; García De Abajo, F. J.; Liz-Marzán, L. M. Seeded Growth of Submicron Au Colloids with Quadrupole Plasmon Resonance Modes. *Langmuir* **2006**, *22*, 7007−7010.

(43) Hastings, S. P.; Swanglap, P.; Qian, Z.; Fang, Y.; Park, S.-J.; Link, S.; Engheta, N.; Fakhraai, Z. Quadrupole-Enhanced Raman Scattering. *ACS Nano* **2014**, *8*, 9025−9034.

(44) He, H.; Xu, X.; Wu, H.; Jin, Y. Enzymatic plasmonic engineering of Ag/Au bimetallic nanoshells and their use for sensitive optical glucose sensing. *Adv. Mater.* **2012**, *24*, 1736−1740.

(45) Zhang, X.; Wei, M.; Lv, B.; Liu, Y.; Liu, X.; Wei, W. Sensitive colorimetric detection of glucose and cholesterol by using Au@Ag core-shell nanoparticles. *RSC Adv.* **2016**, *6*, 35001−35007.